Pflugers Arch - Eur J Physiol (2003) 446:559–571
DOI 10.1007/s00424-003-1077-0

ION CHANNELS, TRANSPORTERS

S. P. Fraser · J. A. Grimes · J. K. J. Diss · D. Stewart · J. O. Dolly · M. B. A. Djamgoz

Predominant expression of Kv1.3 voltage-gated K^+ channel subunit in rat prostate cancer cell lines: electrophysiological, pharmacological and molecular characterisation

Received: 26 November 2002 / Accepted: 24 March 2003 / Published online: 1 July 2003

Abstract Voltage-gated K^+ currents expressed in two rat prostate cancer ('Dunning') cell lines of markedly different metastatic ability were characterised using electrophysiological, pharmacological and molecular approaches. Whole-cell patch-clamp recordings showed that both strongly metastatic MAT-LyLu and weakly metastatic AT-2 cell lines possessed outward (delayed-rectifier type) K^+ currents, which activated at around −40 mV. From the parameters measured, several characteristics of the two cell lines were similar. However, a number of statistically significant differences were noted for MAT-LyLu versus the AT-2 cells as follows: (1) current densities were smaller; (2) the slope factor for channel activation was smaller; (3) the voltage at which current was half-inactivated, and the slope factor for channel inactivation were greater; (4) the time constants for current decay at −20 and 0 mV were smaller; and (5) the residual peak current was larger following 60 s of repetitive voltage pulses for stimulation frequencies in the range 0.05–0.2 Hz. On the other hand, the K^+ currents in both cell lines showed similar pharmacological profiles. Thus, the currents were blocked by 4-aminopyridine, tetraethylammonium, verapamil, margatoxin, and charybdotoxin, with highly similar IC_{50}s for given blockers. The electrophysiological and pharmacological data taken together suggested expression of voltage-gated K^+ channels of the Kv1 family, expression of the Kv1.3 subunit being predominant. Western blot and RT-PCR tests both confirmed that the cells indeed expressed Kv1.3 and to a lesser extent Kv1.4 and Kv1.6 channel α-subunits. In view of the similarity of channel expression in the two cell lines, voltage-gated K^+ channel activity may not be a primary determinant of metastatic potential in the rat model of prostate cancer, but the possible contribution of K^+ channel activity to the metastatic process is discussed.

Keywords Dunning · Ion channels · Kv1.3, Kv1.4, Kv1.6 · Metastasis · Patch-clamp · Potassium · Prostate cancer · RT-PCR

S. P. Fraser (✉) · J. A. Grimes · J. K. J. Diss · D. Stewart · J. O. Dolly · M. B. A. Djamgoz
Department of Biological Sciences,
Imperial College of Science, Technology and Medicine,
Sir Alexander Fleming Building, London, SW7 2AZ, UK
e-mail: s.p.fraser@ic.ac.uk
Tel.: +44-207-5945441
Fax: +44-207-5842056

Introduction

Voltage-gated K^+ channels (VGPCs) contribute to a wide range of cellular functions in both so-called 'excitable' and 'non-excitable' cell types. These functions include control of resting membrane potential (reviewed in [21]); solute and water transport [26]; cell volume regulation [29]; cell adhesion [24]; apoptosis [5] and lymphocyte activation [8]. Many of these processes may have a potential direct involvement in tumour metastasis (i.e. the ability of cells disseminating from a primary tumour to form secondary tumours at distant sites in the body). Voltage-gated ion channels are expressed in cell lines derived from several cancers, including: prostate [19, 27, 28, 51], lung [2], astrocytoma [5] and melanoma [37]. Furthermore, ion channel expression can be controlled by mitogens and oncogenes [3, 4], and their expression can influence several essential characteristics of cancer cells, such as invasion [19, 28, 52], apoptosis [5], lateral motility [12], morphological development [13] and proliferation [5, 14, 51].

We have shown previously that upregulation of functional voltage-gated Na^+ channels (VGSCs) by increased transcription [9] is associated with enhanced metastatic potential in both rat and human prostatic cancer cell lines [12, 19, 27, 52]. Of the rat Dunning model of prostate cancer, the AT-2 cell line is characterised by its very low rate (<10%) of metastasis to non-specific sites, when injected subcutaneously into syngeneic rats (and is thus referred to as 'weakly metastatic'), whilst the MAT-LyLu cell line displays a high rate (>90%) of metastasis specifically to the lungs and lymph

nodes (and is thus referred to as 'strongly metastatic') [22]. These cell lines were found to express VGPCs [19] that appeared to have a differential involvement in proliferation [14]. However, it is not known if there are significant qualitative and/or quantitative differences in the VGPC characteristics of these two contrasting cell lines. In the present study, we have used the whole-cell patch-clamp recording technique, a variety of pharmacological tools and molecular biology to characterise in depth the VGPC(s) of the Kv1 family present in the AT-2 and MAT-LyLu cell lines, in a continued comparative approach to the Dunning model. The overall aim was two-fold: (1) to determine possible differences, if any, between the voltage-gated K^+ currents in the two cell lines; and (2) to gain an insight to the probable molecular nature of the underlying Kv1 channel subunit(s) being expressed.

Materials and methods

Tissue culture and electrophysiological recording

Cell culture and electrophysiological recordings were performed as before [18, 19], but with the following modifications. Patch pipettes (of resistance 5–15 MΩ) were filled with a solution containing (in mM) NaCl (5), KCl (145), $MgCl_2$ (2), $CaCl_2$ (1), HEPES (10) and EGTA (11), adjusted to pH 7.4 with 1 M KOH. The effective intracellular Ca^{2+} concentration was ~15 nM (Patchers Power Tools, WaveMetrics, Ore., USA). Strong buffering of intracellular Ca^{2+} was used to prevent possible activation of a fibroblast-type intermediate-conductance Ca^{2+}-dependent K^+ ('FIK') channel reported to be present in AT2.1 and MAT-LyLu cells [41]. The cells were perfused with an external physiological solution containing (in mM): NaCl (144), KCl (5.4), $MgCl_2$ (1), $CaCl_2$ (2.5), *N*-hydroxyethylpiperazine-*N'*-2-ethanesulfonic acid (5), D-glucose (5.6), adjusted to pH 7.2 with 1 mM NaOH. Whole-cell membrane currents were recorded from cells that appeared 'isolated' in culture using an Axopatch 200B (Axon Instruments, Foster City, Calif., USA) amplifier. The amplifier was used to compensate series resistance by ~80% and junction potential errors were minimised by use of a 3-M KCl agar bridge. Analogue signals were filtered at 5 kHz using a lowpass Bessel filter. Signals were sampled at 50 kHz and digitised using a Digidata (1200) interface. Data acquisition and analysis of whole-cell currents were performed using pClamp software (Axon Instruments). All recordings were made in the presence of 1 μM tetrodotoxin (TTX) to block VGSCs completely [19], and unless indicated otherwise, the holding potential was −90 mV.

Standard voltage-clamp protocols were used to study the electrophysiological and pharmacological properties of the K^+ currents. Specific details are given in the Results, the individual figure legends or have been explained previously [18, 19].

Pharmacological solutions

Various pharmacological agents, including tetraethylammonium (TEA), 4-aminopyridine (4-AP), verapamil, margatoxin (MGTX) and charybdotoxin (CTX) were tested for their effects on the K^+ currents. Most drug solutions were made by direct addition to the control external bathing solution. However, TEA solutions were made by equimolar substitution of TEA-Cl for NaCl. Solutions of expensive drugs (e.g. CTX) were applied using a 'puffer' [14]. All chemicals were obtained from Sigma Chemicals (Poole, Dorset, UK), except MGTX and CTX, which were supplied by Alomone Labs (Jerusalem, Israel).

Analysis of membrane currents

Leak current subtraction was performed as described previously [18]. Equations used to calculate membrane conductance, reversal potential, steady-state activation/inactivation parameters, and the time-course of current inactivation or recovery from inactivation were as described previously [18], with the following additions:

1. The kinetics of the total current flowing during a voltage step were calculated using a Hodgkin-Huxley 'n^4h' equation of the form:

$$I = I_{max}[1 - \exp(-t/\tau_a)]^4 \exp(-t/\tau_i) \quad (1)$$

where I_{max} is the maximum current at a given potential; and τ_a and τ_i are time constants of current activation and inactivation, respectively.

2. The voltage dependence of the time constant (τ) of activation was described by a single exponential function of the form:

$$\tau = A_1 + A_2 \exp(-V/V_0) \quad (2)$$

where A_1 is a constant and A_2 is a coefficient of decline of τ with voltage; V is the membrane potential; and V_o is a constant describing the voltage dependence of τ.

3. Pharmacological dose-response data were fitted to a Langmuir adsorption isotherm or Hill equation of the form:

$$B = M/[1 + (IC_{50}/[D])] \quad (3)$$

where B is the block at a given drug concentration ($[D]$); M is the block caused by a saturating concentration of the drug; and IC_{50} is the concentration of the drug at which 50% of the current was blocked.

Western blots

K+ channel antibodies

VGPC proteins were detected using antibodies specific for individual Kv1 α-subunits [1, 49, 50]. mAb5 and the Kv1.5 antibody were monoclonals raised in mice against, respectively, the Kv1.2 α-subunit purified from bovine brain and a synthetic peptide to amino acids 542–602 of Kv1.5 [1, 49]. All other K^+ channel antibodies were polyclonal, raised in rabbits against glutathione-S-transferase fusion proteins containing C-terminal regions of cloned Kv channel proteins [50]. Secondary antibodies were horseradish peroxidase (HRP)-conjugated anti-mouse (for monoclonals) or anti-rabbit (for polyclonals) immunoglobulins.

Preparation of samples and determination of protein content

Membrane preparations were made by homogenising rat brain or pelleted cultured cells as described previously [50]. Phenylmethylsulfonyl fluoride (1 mM) was added to solutions at all stages of sample preparation, to prevent proteolytic degradation of the antigens, and all samples were sonicated in a vibrating probe sonicator for 10 s prior to the subsequent steps. The protein content of each sample was determined using the colorimetric BCA kit (Pierce & Warriner [UK], Chester, UK), according to the manufacturer's instructions.

SDS-PAGE and Western blotting

Protein samples were diluted in SDS sample buffer containing 5% β-mercaptoethanol to concentrations of 1–10 mg/ml, and 5% bromophenol blue was added. Samples were then loaded onto 10% polyacrylamide gels. The amount of protein loaded in each case has

been specified in the corresponding figure legend. After electrophoresis, proteins were transferred from gels onto Hybond-C extra nitrocellulose membrane (Amersham Pharmacia Biotech, Bucks, UK) using a BioRad Transblot apparatus. Prior to antibody labelling, nitrocellulose membranes were incubated in blocking buffer, a solution of 5% low-fat powdered milk and 0.2% Tween 20 in PBS for 2 h at 22°C. Primary antibodies were diluted 1:500 in blocking buffer and used to probe protein blots by incubation for 1 h at 22°C. Secondary antibodies were diluted 1:10,000 in blocking buffer and incubated as for primary antibodies. Blots were washed for 1 h in six changes of NP40 or TBST washing solution after both primary and secondary antibody incubations. Finally, blots were washed three times in PBS to remove detergent, and antibody labelling was visualised using the ECL detection system (Amersham Pharmacia Biotech).

RT-PCR

RNA was extracted from MAT-LyLu and AT-2 cells, and from adult Copenhagen rat brain tissue, using the guanidium thiocyanate-acid phenol method [7]. Genomic DNA was removed from the extracts by digestion with DNase I (Amersham Pharmacia Biotech) and 5 μg of the resultant total RNA was used as the template for single-stranded cDNA (sscDNA) synthesis (Superscript II, Life Technologies, Paisley, UK). sscDNA was primed with a random hexamer primer mix (Amersham Pharmacia Biotech) in a final volume of 20 μl. PCR using specific 20mer primers for rat Kv1.3, Kv1.4, Kv1.5 and Kv1.6 K^+ channel α-subunits was then performed. The primers used amplified nucleotides 666–1184; 1528–1943; 1071–1645; 922–1342, for Kv1.3 (64°C), Kv1.4 (60°C), Kv1.5 (62°C) and Kv1.6 (60°C), respectively (numbering according to GenBank; reaction annealing temperature used indicated in parentheses). Two additional 20mer primers were also used in order to sequence the S5-S6 pore region of the Kv1.3 α-subunit. These primers amplified nucleotides 1483–1954 (reaction annealing temperature, 60°C).

Reactions were performed on 2.5 μl of the synthesised sscDNA, using 200 μM of each dNTP (Amersham Pharmacia Biotech), 1 unit of Taq DNA polymerase (Amersham Pharmacia Biotech), 1× Taq buffer and 0.5 μM of each primer, in a final volume of 20 μl as follows: 94°C for 5 min; 1 U enzyme added; 94°C for 1 min; 60–64°C for 1 min; 72°C for 1 min, with the main section repeated 30–50 times (depending on the reaction). Control PCRs were performed in which the sscDNA template was replaced with water or an aliquot from a reverse transcription reaction which had no reverse transcriptase added. All products were analysed by gel electrophoresis on 0.8% agarose gels and then were gel purified and ligated into the pGEM T-vector (Promega pGEM T-vector System). This was then used to transform *E. coli* (pMosBlue, Amersham Pharmacia Biotech). Plasmid DNA was recovered from bacterial cell cultures and resultant clones were sequenced using the Vistra DNA 725 automated sequencer.

Semi-quantitative RT-PCRs were performed using a kinetic observation approach as described before [9]. The specific Kv1.3 PCR described above was used (amplifying nucleotides 666–1184), except that reactions were performed in a final volume of 60 μl and each reaction was seeded with 2.4 μl of sscDNA (standard concentrations of Taq buffer and dNTPs; 3 units of Taq polymerase). All reactions were performed simultaneously with control PCRs (no template or no reverse-transcriptase added-sscDNA). 5 μl aliquots of the 60-μl reaction were taken at the end of successive amplification cycles, for 11 cycles, while reactions were held at 72°C, were electrophoresed and photographed using the GDS 7500 Advanced Gel Documentation System (Ultra-Violet Products).

NADH:cytochrome b5 reductase ($rCytb_5R$), found to be expressed at very similar levels in normal and cancerous cells [9, 11, 34], was used to control for any effects of possible variations in quality and quantity of the initial RNA, efficiency of the reverse-transcription and amplification between samples. $rCytb_5R$ 20-mer primers amplified nucleotides 385–809 (annealing temperature 60°C for both).

GenBank sequence nucleotide numbers

Nucleotide numbering was according to GenBank/EMBL Data Bank accession numbers M31744, X16002, M27158, M27159 and D00636, for Kv1.3, Kv1.4, Kv1.5, Kv1.6 and $rCytb_5R$, respectively. The sequences have been submitted to the GenBank/EMBL Data Bank with the following accession numbers: AJ276138, AJ276135, AJ276136 and AJ276137 for rat brain Kv1.3, MAT-LyLu Kv1.3, AT-2 Kv1.3, and MAT-LyLu Kv1.6, respectively.

Table 1 Summary of electrophysiological and pharmacological data comparing the voltage–gated K^+channels expressed in AT–2 and MAT–LyLu cell lines. Data are presented as mean±SEM (*4-AP* 4-aminopyridine,*CTX* charybdotoxin, *MGTX*margatoxin, *TEA* tetraethylammonium). *NS* No statistical difference between the parameters

Characteristic	AT-2	MAT-LyLu	Statistical significance
Resting potential (mV)	−58.3±3.3	−72.9±2.6	**
Capacitance (pF)	33.7±3.0	29.1±2.1	NS
Activation voltage (mV)	−38.2±1.6	−40.2±1.9	NS
Maximum current (pA)	711±43	427±33	**
Current density (pA/pF)	21.4±1.2	14.8±1.1	**
$V_{1/2}$ activation (mV)	−23.3±0.5	−24.0±0.4	NS
k activation (mV)	7.1±0.4	5.9±0.4	*
τ_a voltage dependence (mV)	13.7±0.4	13.1±0.4	NS
$V_{1/2}$ inactivation (mV)	−33.9±0.1	38.4±0.2	*
k inactivation (mV)	−3.7±0.1	−5.1±0.2	*
Time constant of current decay at –20 mV (ms)	1190±270	720±90	*
Time constant of current decay at 0 mV (ms)	600±70	490±25	*
Relative current (0.05 Hz for 60 s)	0.87±0.04	0.99±0.03	**
Relative current (0.1 Hz for 60 s)	0.66±0.02	0.79±0.05	**
Relative current (0.2 Hz for 44 s)	0.54±0.01	0.6±0.03	*
TEA IC_{50} (mM)	9±2	11±5	NS
4–AP IC_{50} (mM)	4±2	1±1	NS
Verapamil IC_{50} (μM)	19±2	18±2	NS
% MGTX block (5×10^{-7} M)	53±5	64±6	NS
% CTX block (4.5×10^{-7} M)	67±8	58±10	NS
% MGTX (5×10^{-8} M)+CTX block (4.5×10^{-8} M)	82±4	85±3	NS

* Statistical significance at $P<0.05$
** Statistical significance at $P<0.01$

Data analysis

All data values were calculated as mean±SEM. Statistical comparisons between data sets were performed using either paired or unpaired Student's *t*-tests, where appropriate, using the Statworks version 1.1 software package (Cricket Software, UK). Differences were considered statistically significant for $P<0.05$ (*) or $P<0.01$ (**).

Results

The quantitative electrophysiological and pharmacological data obtained from the two cell lines and their statistical analyses are summarised in Table 1.

General electrophysiological properties

The resting potentials of the AT-2 and MAT-LyLu cells, recorded immediately after achieving the whole-cell configuration, were −58.3±3.3 mV (n=62) and −72.9±2.6 mV (n=76; $p<0.01$); whole-cell capacitances were 33.7±3.0 pF and 29.1±2.1 pF, respectively ($P>0.05$). These characteristics, as well as the voltage-gated current amplitudes in either cell type did not change during the experimental period (1–4 days in culture; data not shown).

Activation

Depolarisation of either cell type, from a holding potential of −90 mV to between –60 mV and +60 mV, with an interpulse period of 20 s, elicited outward currents which rapidly reached a peak and decayed slowly (Fig. 1A, B). A shorter interpulse period of 2 s resulted in smaller currents, probably due to a lack of recovery from inactivation in between successive pulses (not shown). Currents activated at −38.2±1.6 mV in AT-2 and −40.2±1.9 mV in MAT-LyLu cells ($P>0.05$; n=50 each). At +60 mV, the peak current amplitude was 711±43 pA (n=185) in the AT-2 cells, and 427±33 pA (n=179) in the MAT-LyLu cells, corresponding to current densities of 21.4±1.2 pA/pF and 14.8±1.1 pA/pF, respectively. The maximum current size and current density were significantly smaller in the MAT-LyLu compared with the AT-2 cell line ($P<0.01$ for both).

At voltages above activation threshold, conductance rose steeply before reaching a plateau at ~0 mV, whereupon further depolarisation caused no increase in conductance (Fig. 1C). Fitting the data to a Boltzmann function gave $V_{1/2}$ values of −23.3±0.5 mV and −24.0±0.4 mV ($P>0.2$), and k_a values of 7.1±0.4 mV and 5.9±0.4 mV per *e*-fold increase in conductance ($P<0.05$), for the AT-2 and MAT-LyLu cells, respectively (n=10 each).

At +60 mV, the outward currents reached their peak 10.5±2.4 ms and 10.9±2.8 ms after the onset of the voltage pulse for the AT-2 and MAT-LyLu cells, respectively (n=20 each). For both cell types, the kinetics of activation during a 200-ms pulse became progressively faster with increasing depolarisation. At +60 mV, the activation time constant (τ_a) had values of 1.1±0.1 ms and 0.9±0.5 ms for the AT-2 and MAT-LyLu cells ($P>0.05$ and n=5), whilst at −20 mV the values were 8.8±0.3 ms and 7.7±0.2 ms ($P>0.05$ and n=5). The values of τ_a at –20 mV and –60 mV were significantly different for both cell lines ($P<0.01$ for both). The voltage dependence of τ_a was described by coefficients with values of 13.7±0.4 mV and 13.1±0.4 mV per *e*-fold increase in activation rate for the AT-2 and MAT-LyLu cells, respectively ($P>0.05$).

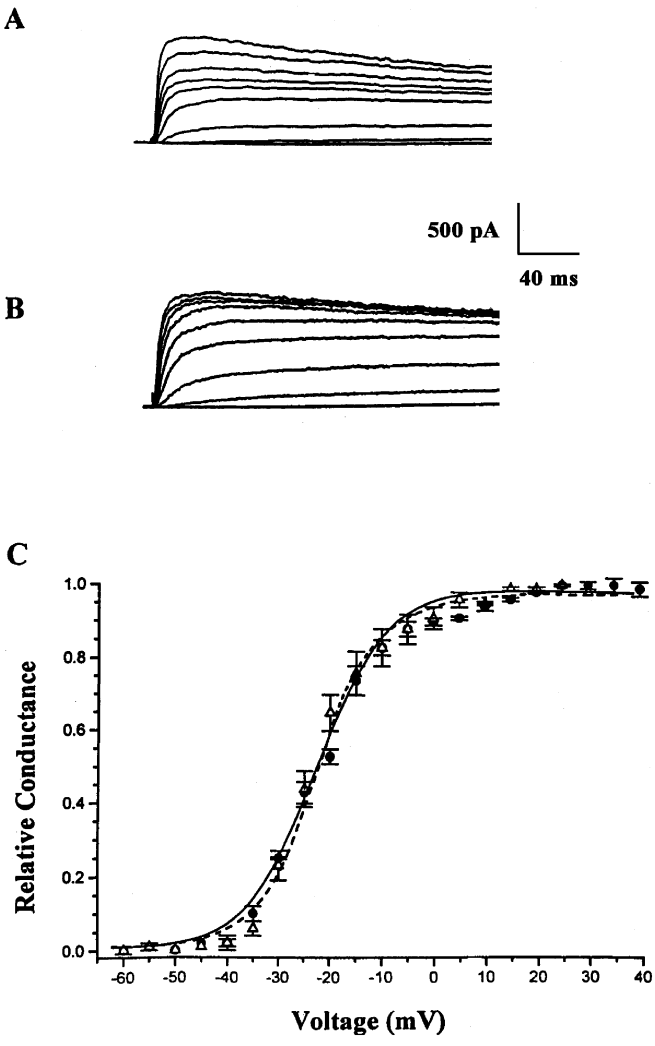

Fig. 1 Typical families of outward currents (**A**, **B**) from AT-2 and MAT-LyLu cells. Cells were pulsed from a holding potential of –90 mV to test potentials between −60 and +60 mV in 5-mV increments. Voltage pulses were applied with a repeat interval of 20 s. **C** Voltage dependence of conductance measured in AT-2 (*filled circles*, *dashed line*) and MAT-LyLu (*open triangles*, *solid line*) cells. Peak currents were converted to conductance, normalised relative to peak value for each cell and plotted as mean±SEM (n=10). *Lines* represent fits to a Boltzmann function. Scale bar applies to both **A** and **B**

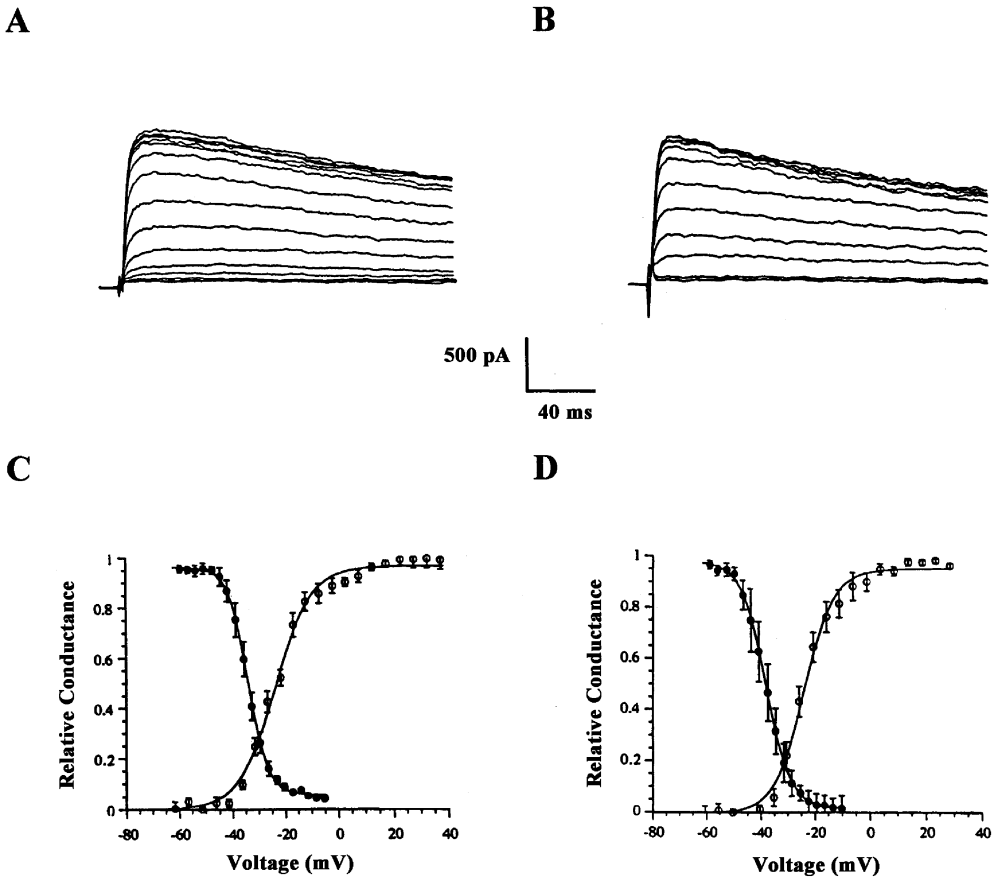

Fig. 2 Typical recordings of the voltage-dependence of steady-state inactivation of the outward currents for AT-2 (**A**) and MAT-LyLu (**B**) cells. Cells were pre-pulsed for 5 s over the range of membrane potentials from –60 mV to –5 mV in 5-mV steps prior to applying a constant test pulse to +60 mV. Voltage pulses were applied with a repeat interval of 2 min. Scale bar applies to both **A** and **B**. Relationship between activation (*open circles*) and steady state inactivation (*filled circles*) and membrane voltage were plotted on the same axis for AT-2 (**C**) and MAT-LyLu (**D**) cells. Data points represent mean±-SEM (n=5). The curves were derived by fitting the data to Boltzmann functions

Inactivation

The voltage dependence of steady-state inactivation was studied (Fig. 2A, B). For both cell types, the test pulse current was maximal for the most hyperpolarised pre-pulse potentials, and then declined as the pre-pulse became more depolarised (Fig. 2C, D). Fitting the data to a Boltzmann function gave the following values: $V_{1/2}$=–33.9±0.1 mV and –38.4±0.2 mV; and k_i=–3.7±0.1 mV and –5.1±0.2 mV per *e*-fold change in current for the AT-2 and MAT-LyLu cells, respectively (n=5 each). Both $V_{1/2}$ and k_i were significantly different between the two cell types (P<0.05). Comparison of the steady-state activation and inactivation relationships for each cell type revealed 'window currents' that were comparable (Fig. 2C, D).

The decay time-course of the current could be fitted by a single exponential function [18] for both cell lines and appeared to be largely independent of voltage in the range 20–60 mV. However, inactivation was significantly slower at more negative voltages. For example, the time constants for current decay at 60 mV were 440±20 ms and 500±70 ms, whilst at –20 mV these were 1190±270 ms and 720±90 ms for the AT-2 and MAT-LyLu cell lines, respectively (p<0.05 for comparison of 60 mV versus –20 mV, for both cell lines). In addition, the time constant was significantly larger at –20 mV and 0 mV for the AT-2 compared with the MAT-LyLu cell line (Table 1; P<0.05 for both voltages).

In response to repetitive voltage pulses (–90 mV to +60 mV), over a frequency range 0.05–2 Hz, the current amplitude decreased for both cell lines (not shown). Both the time-course of this 'current rundown' and the final reduction in peak current over 60 s increased with stimulation frequency. However, the residual peak current was larger for the MAT-LyLu cell line, in comparison to the AT-2 cell line, for stimulation frequencies in the range 0.05–0.2 Hz (see Table 1). Measurement of the current at the end of a given (nth) pulse in comparison to the peak current of the following (nth+1) pulse showed that current peak for a given voltage pulse was never smaller than the current elicited by the preceding pulse, indicating that there was no continuation of the inactivation process between successive pulses. These experiments also revealed that at least 20 s were needed for full recovery from the inactivation induced by a 200-ms voltage pulse to +60 mV.

Ionic selectivity

The reversal potentials of the currents were determined by tail current analysis for 4.5, 29 and 145 mM external K^+. The Nernst equation gave values of 47.7±0.3 mV and

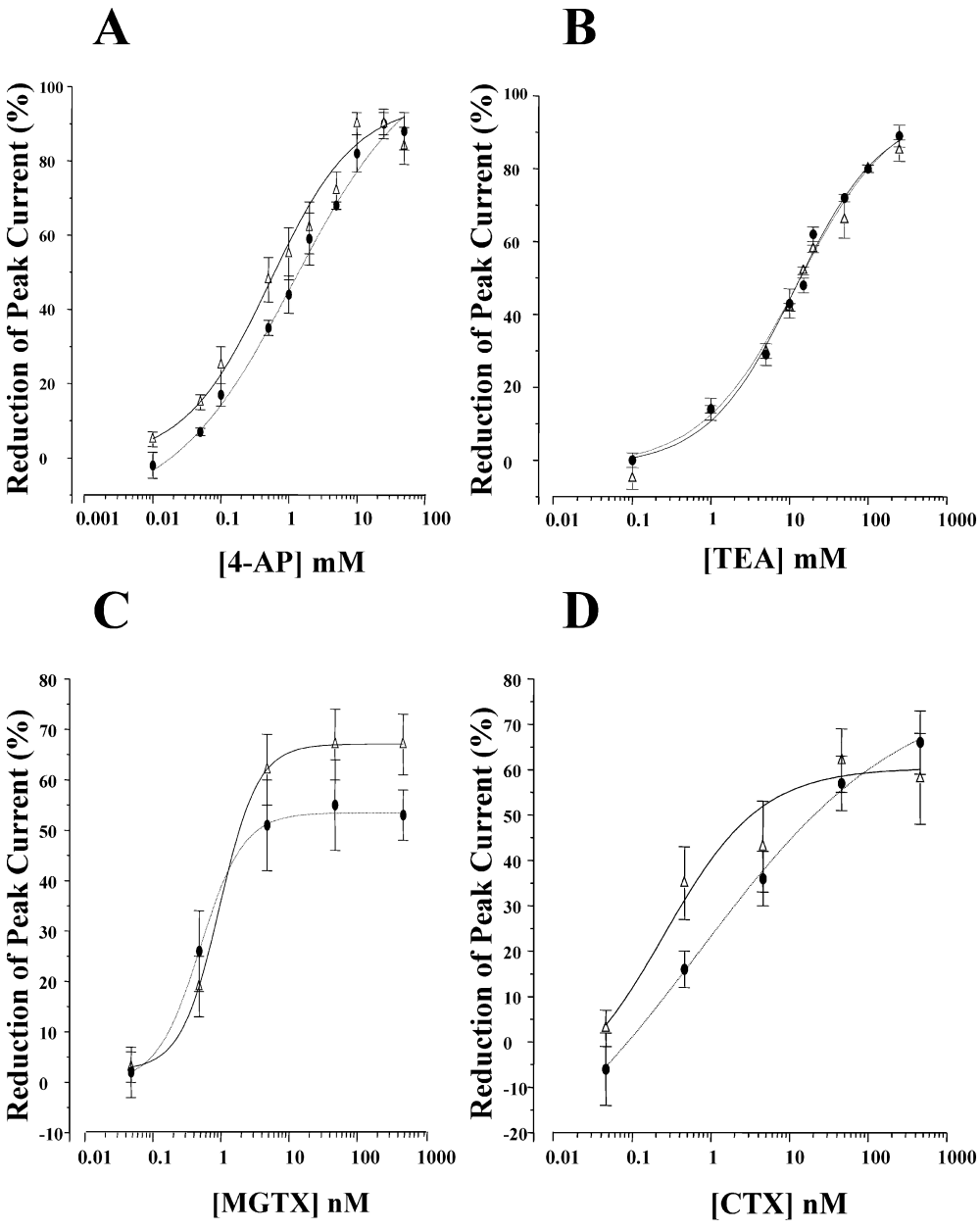

Fig. 3 Averaged dose-response curves for **A** 4-AP, **B** TEA, **C** margatoxin (MGTX) and **D** charybdotoxin (CTX) in AT-2 (*filled circles*, *dashed line*) and MAT-LyLu (*open triangles*, *solid line*) cells. The percentage reduction of the peak current at +60 mV was plotted as a function of the drug concentration. Data are plotted as mean±SEM (n>5 for each concentration). *Lines* represent fits to the Lamgmuir adsorption isotherm

48.6±0.5 mV change in reversal potential per tenfold change in external K^+ concentration for AT-2 and MAT-LyLu cells, respectively (P>0.05; n=5 for each cell line). Replacing 145 mM Na^+ with equimolar choline had no effect on current reversal, whilst replacing internal K^+ with Cs^+ totally abolished all outward currents (n=5 for each cell line). Substituting Mn^{2+} for external Ca^{2+} had no effect on the currents and application of the Ca^{2+} ionophore A23187 (10 μM) for 2 min also had no effect on the currents (n=5 for each cell line; not shown).

Pharmacology

4-AP

The outward currents were blocked by 4-AP in a dose-dependent manner (Fig. 3A). The IC_{50} values for the peak currents were 4±2 mM and 1±1 mM for the AT-2 and MAT-LyLu cells, respectively (P>0.2; n>4 for each concentration).

TEA

The amplitude of the peak outward current was reduced in both cell lines by TEA (Fig. 3B). The effect was dose dependent with IC_{50} values of 9±2 mM and 11±5 mM for

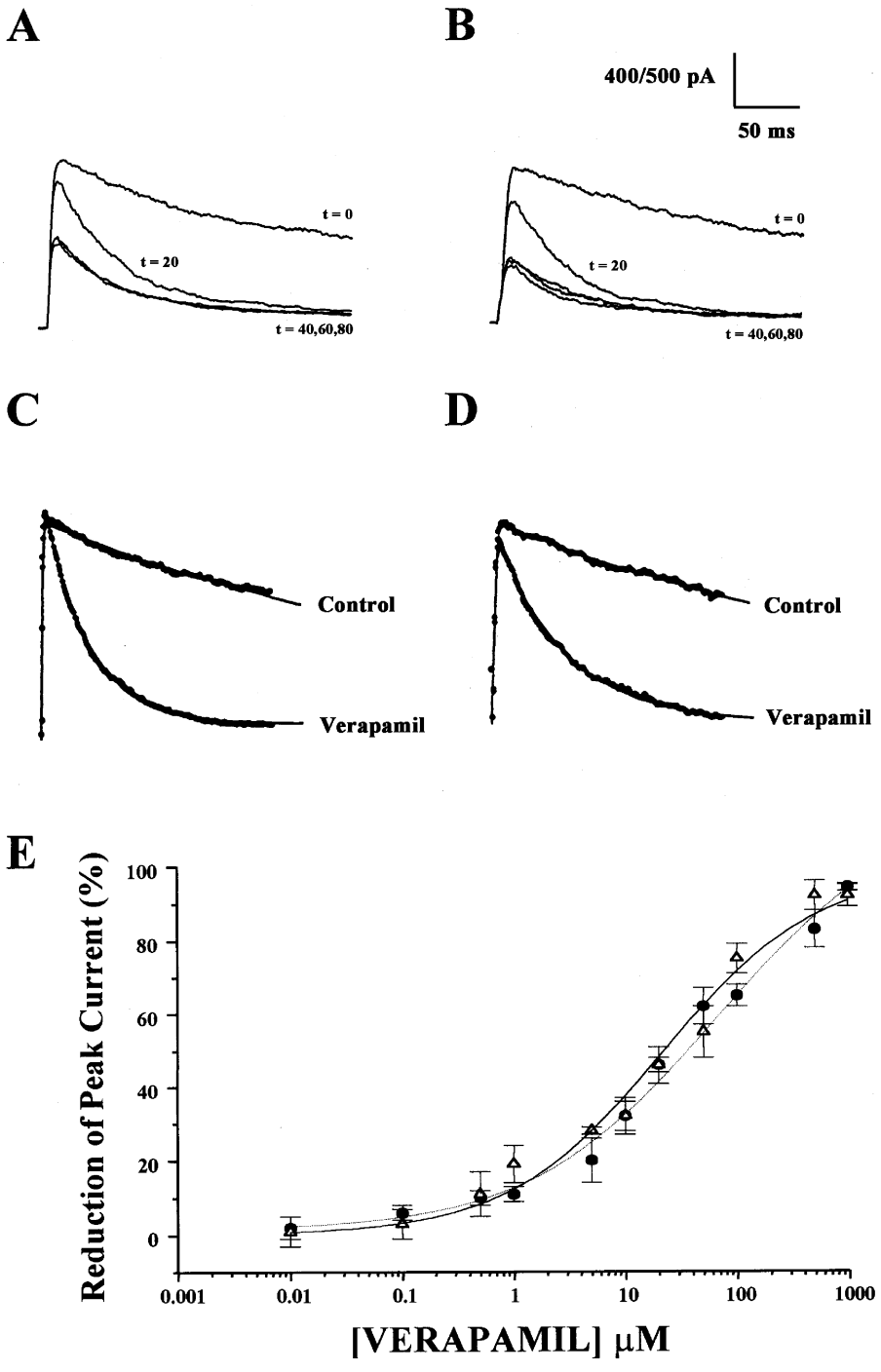

Fig. 4 Typical outward currents recorded in the AT-2 (**A**) and MAT-LyLu (**B**) cells before and after application of 20 μM verapamil. Cells were depolarised from –90 to +60 mV for 200 ms with a repeat interval of 20 s. Traces before (t=0) and at 20, 40, 60 and 80 s following 20 μM verapamil application. Scale bar applies to both **A** (400 pA) and **B** (500 pA). Effect of 20 μM verapamil on the current elicited by a single voltage pulse from –90 to +60 mV for 200 ms in AT-2 (**C**) and MAT-LyLu (**D**) cells (n>6 for both cell types). *Lines* represent fits to a Hodgkin-Huxley 'n^4h' model. Values of the time constants for current activation and decay for the traces presented are as follows: **C** Control: τ_a=1.1 ms and τ_i=435.5 ms; verapamil: τ_a=1.2 ms and τ_i=36.3 ms. **D** Control: τ_a=1.5 ms and τ_i=420.4 ms; verapamil: τ_a=1.5 ms and τ_i=60.6 ms. **E** Averaged dose-response curve for verapamil in AT-2 (*filled circles*, *dashed line*) and MAT-LyLu (*open triangles*, *solid line*) cells. The percentage reduction of the peak current at +60 mV was plotted as a function of verapamil concentration. Data are plotted as mean±SEM) (n>4 for each concentration). *Lines* represent fits to the Lamgmuir adsorption isotherm

the AT-2 and MAT-LyLu cells, respectively (P>0.2; n>4 for all concentrations and for both cell types). TEA also slowed the current decay. In the control solution, the current decayed 45.1±3.7% for the AT-2 cells and 43.7±4.1% for the MAT-LyLu cells over the 200-ms stimulation period (P>0.05; n=5). In the presence of 20 mM TEA, however, the current decays were reduced significantly to 24.3±3.1% and 23.6±2.9%, respectively (n=5; P<0.01 cf. respective control; P>0.05 comparing the two cell lines).

MGTX

The outward currents in both cell lines were blocked in a dose-dependent manner by MGTX (Fig. 3C). However, there was a large variability in the percentage block of the peak current for given concentrations of MGTX on individual cells. In addition, blockage appeared to saturate at 5×10^{-9} M, which suppressed the currents in the AT-2 cells by 51±9% and in the MAT-LyLu cells by 62±7%; these values were not significantly different to

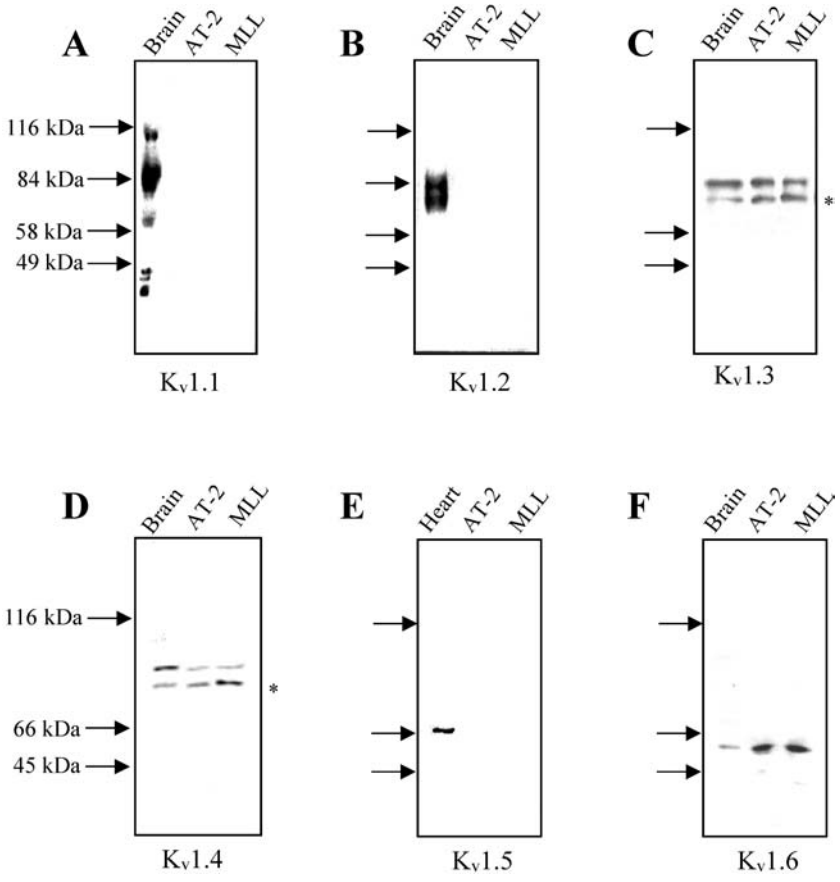

Fig. 5 Expression of **A** Kv1.1, **B** Kv1.2, **C** Kv1.3, **D** Kv1.4 **E** Kv1.5 and **F** Kv1.6 voltage-gated K^+ channel α-subunits in AT-2 and MAT-LyLu cells studied by Western blot. Each cell extract comprised 50 μg of AT-2 and MAT-LyLu membrane preparations, whilst the rat brain and rat heart controls were 10 μg. Blots were incubated with 5 μg/ml of the anti-channel primary antibodies, and horseradish peroxidase-conjugated anti-rabbit (for anti-Kv1.1, anti-Kv1.3, anti-Kv1.4 and anti-Kv1.6) or anti-mouse (for anti-Kv1.2 and anti-Kv1.5) secondary antibodies. Blots were visualised using the ECL detection method and were repeated at least three times. Western blots indicated that Kv1.3, Kv1.4 and Kv1.6 subunits were expressed in the AT-2 and MAT-LyLu cell lines. An *asterisk* indicates partially degraded protein or possible non-glycosylated populations [33]

the blockage induced by 5×10^{-7} M MGTX (53±5% and 64±6%, respectively; $P>0.05$ for both comparisons).

CTX

The outward currents in both cell lines were also blocked by CTX in a dose-dependent manner (Fig. 3D). As for the effect with MGTX, there was a large variation in the responses of the cells to given CTX concentrations. Effects appeared to saturate at 4.5×10^{-8} M, which blocked the currents in the AT-2 cells by 56±8% and the MAT-LyLu cells by 62±7%; these values were not significantly different to the blockages induced by 4.5×10^{-7} M CTX (67±8% and 58±10%, respectively; $P>0.05$ for both comparisons). Combined application of 4.5×10^{-8} M CTX and 5×10^{-8} M MGTX blocked the currents further, in the AT-2 cells by 82±4% ($n=6$) and the MAT-LyLu cells by 85±3% ($n=6$). These values were not significantly different to each other ($P=0.5$) but were significantly greater than the blockages induced by individual application of 4.5×10^{-8} M CTX or 5×10^{-8} M MGTX to either cell line ($P<0.05$ for all comparisons). However, this combined effect appeared to be maximal since, for example, co-application of 1.15×10^{-6} M CTX and 1.3×10^{-6} M MGTX blocked the VGPCs in the MAT-LyLu cells by 78±3% ($n=4$). This value was no different from the combined application of 4.5×10^{-8} M CTX and 5×10^{-8} M MGTX for this cell line ($P=0.09$).

Verapamil

Application of verapamil had two distinct effects on the outward currents; a reduction in peak amplitude (Fig. 4A, B) and alteration in inactivation kinetics (Fig. 4C, D). The effect of verapamil was dose dependent with IC_{50}s of 19±2 μM and 18±2 μM for the AT-2 and MAT-LyLu cells, respectively ($P>0.05$; $n>5$ for each concentration; Fig. 4E). For both cell lines, immediately following verapamil application, the activated current decayed rapidly to a lower level and subsequent pulses (presented after 40 s or later) produced smaller currents (Fig. 4A, B). For the AT-2 cells, the activation time constants for a 200-ms pulse (from −90 mV to +60 mV) were 0.8±0.1 ms in the control solution and 0.8±0.1 ms in the presence of 20 μM verapamil ($P=0.90$; $n=5$). For the MAT-LyLu cells, the activation time constant was 1.5±0.3 ms in the control solution and 1.5±0.2 ms in the presence of 20 μM verapamil ($P=0.98$; $n=5$). In contrast, the inactivation time constants were significantly reduced by 20 μM verapamil, falling from 366.4±37.0 ms to 22.5±4.3 ms in AT-2 cells, and from 417.7±63.3 ms to 43.6±5.0 ms in the MAT-LyLu cells ($P<0.01$ and $n=5$ for both cell lines).

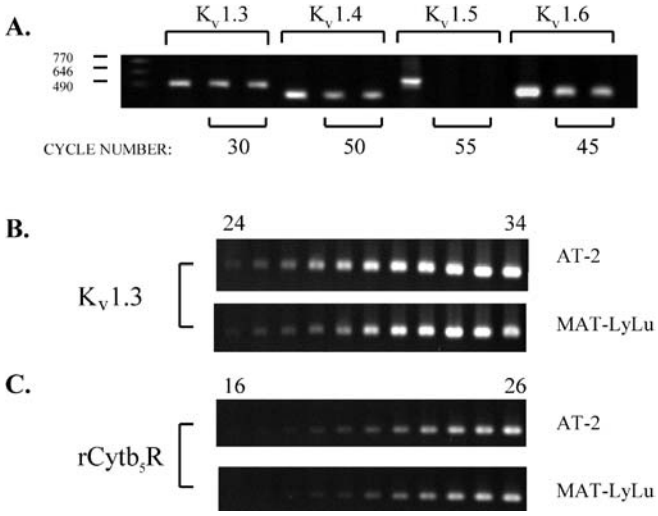

Fig. 6A–C Gel images of RT-PCR tests performed on cDNA derived from AT-2 and MAT-LyLu cell lines and rat brain. **A** RT-PCR tests for Kv1.3, Kv1.4, Kv1.5 and Kv1.6 α-subunits. For each test the three lanes on the electrophoresis gel represent products obtained from rat brain, AT-2 and MAT-LyLu cDNAs, from left to right, respectively. PCR cycles used in each test are indicated for AT-2 and MAT-LyLu cell lines. For brain cDNA, products were obtained following 30, 35, 40 and 40 cycles for Kv1.3, Kv1.4, Kv1.5 and Kv1.6 tests, respectively. Products were 518 nt, 416 nt, 575 nt and 421 nt for Kv1.3, Kv1.4, Kv1.5 and Kv1.6 tests. Marker bands of 770 nt, 646 nt and 490 nt are shown on the left. Control PCRs (performed on 'no template' or 'no reverse-transcriptase added'-sscDNA) did not yield evident products (not shown). **B** SQT-PCR gel images for Kv1.3 and **C** the $rCytb_5R$ control. Cycle numbers are indicated above the gels

Western blots

Since the electrophysiological and pharmacological data revealed delayed-rectifier type K^+ channels from the Kv1 family, the molecular approaches concentrated on elucidating which members of this family were expressed.

Antibodies directed against Kv1.1, 1.2, 1.3, 1.4, 1.5 and 1.6 α-subunits were tested against membrane preparations from the AT-2 and MAT-LyLu cells (Fig. 5). Kv1.1, 1.2 and 1.5 α-subunits were present only in the brain or heart (Fig. 5A, B, E), whilst Kv1.3, 1.4 and 1.6 were also detected in the cell lines (Fig. 5C, D, F). The anti-Kv1.3 antibody gave bands of ~84 kDa in brain and cell extracts, whilst the anti-Kv1.4 antibody revealed a distinct band of ~90 kDa in both cell lines and brain (Fig. 5D). A lower molecular weight band was also apparent for both cell lines and the brain extract for both anti-Kv1.3 and 1.4 antibody (Fig. 5C, D). The anti-Kv1.6 antibody revealed a faint band of ~60 kDa in brain and stronger bands in AT-2 and MAT-LyLu cell extracts (Fig. 5F).

Reverse transcription PCR

The molecular nature of the Kv1 α-subunit(s) expressed was investigated further by RT-PCR and DNA sequencing. As shown in Fig. 6A, products representing Kv1.3, 1.4 and 1.6 α-subunits were amplified from both MAT-LyLu and AT-2 extracts. No Kv1.5 mRNA was detected in these cell lines, even after 55 amplification cycles, although Kv1.5 products were obtained (and sequenced) from rat brain tissue using the same specific PCR primers (Fig. 6A).

Kv1.3 α-subunit was amplified from both cell lines and rat brain tissue after 30 amplification cycles (Fig. 6A). Semi-quantitative PCR data (Fig. 6B) indicated that Kv1.3 mRNA was expressed (1) at comparable levels in the AT-2 and MAT-LyLu cells, and (2) at a higher level in brain tissue than in either cell line. Kv1.4 and 1.6 products were also more readily amplified from rat brain compared with the cell lines in the specific PCR tests (Kv1.4:35 cycles versus 50 cycles; and Kv1.6:40 cycles versus 45 cycles). This difference was considerably greater for Kv1.4, indicating a low level of expression of Kv1.4 mRNA in the AT-2 and MAT-LyLu cells compared to rat brain.

From sequence data, the Kv1.3 α-subunit (26 amino acids from the start of the amino terminus to the end of S1 and from the end of S4 to 43 amino acids from the end of the carboxyl tail) was identical in both the cell lines and the rat brain. An additional PCR product which spanned the S5-S6 pore region of the Kv1.3 α-subunit was also obtained. The sequence of this product was identical to the published Kv1.3 sequence [55].

The Kv1.4 and Kv1.5 α-subunit sequences obtained from the two rat cell lines and rat brain were identical to the published sequences [54, 55]. The Kv1.6 α-subunit, amplified from all three different sources was identical to the published sequence [55] except in the MAT-LyLu cell line at position 1263 (C to T). However, this is a conservative nucleotide substitution that would not bring about an amino acid change and may represent a polymorphic site.

Discussion

For both cell lines, a shift in reversal potential of ~48 mV per tenfold change in extracellular K^+ concentration was observed, suggesting K^+ as the major permeant ion of the channel. The discrepancy between this and the predicted value of 58 mV has been reported previously [15, 20] and may be due to uncertainties in the assumption of the activity coefficients and/or their possible change under the relevant experimental conditions. Overall, there were limited quantitative differences between the VGPCs expressed in the AT-2 and the MAT-LyLu cells (Table 1), despite the marked contrast in the cells' metastatic character. Within the Kv1 family of VGPCs, the electrophysiological, pharmacological and molecular data taken together were consistent with the majority of VGPCs expressed in the two cell lines comprising the Kv1.3, and to a lesser extent the Kv1.4 and Kv1.6 α-subunits, as discussed in detail in the following sections.

Activation characteristics

The VGPCs of both cell lines activated at around −40 mV with $V_{1/2}$ values of −23 mVand −24 mV and slope factors (k_a) of 7.1±0.4 and 5.9±0.4, respectively. These activation characteristics are most similar to those reported previously for Kv1.3 [10, 54].

Inactivation characteristics

The voltages at which the currents half-inactivated ($V_{1/2}$) were around −34 mV and −38 mV, and k_i values were 3.7 mV and 5.1 mV per *e*-fold change in conductance for AT-2 and MAT-LyLu cells, respectively. Both parameters were significantly different between the cell lines. The decay time-courses of AT-2 and MAT-LyLu K^+ currents were described by a single exponential function with a time constant largely independent of voltage. This is similar to Kv1.3 current decay [10]. In addition, there was significant cellular difference in the time-courses of current decay at two voltages (-20 mV and 0 mV). Although it is possible at these voltages that inactivation was mixed with activation, the observed cellular difference in the inactivation characteristics could reflect differential phosphorylation [25], redox state [47], phospholipid environment [36] or β-subunit coupling [44].

The K^+ currents in both cell lines displayed two major characteristics of C-type inactivation: (1) external application of TEA decreased the inactivation rate; and (2) the currents displayed cumulative inactivation [25]. In contrast, there was no evidence of cumulative inactivation during the interpulse period, suggesting that neither cell type has N-type inactivation [47]. Kv1.3 channels are known to inactivate by a C-type mechanism [25, 35]. Thus, when considering both the mechanism of inactivation, as well as its time-course, Kv1.3 expression appears to be dominant in both AT-2 and MAT-LyLu cells. Although a single Kv1.4 subunit in a hetero-tetramer is capable of promoting N-type inactivation [40], this was never observed. A possible explanation for this is the presence of Kv1.6, which has been shown to prevent N-type inactivation [45].

Pharmacology

4-Aminopyridine

In AT-2 and MAT-LyLu cells, 4-AP caused a dose-dependent reduction of outward current, with half-inhibition occurring at 3.8 and 1.1 mM, respectively. This level of sensitivity is most similar to that of Kv1.3 (IC_{50}~1.5 mM), rather than Kv1.4 (IC_{50}~12.5 mM) or Kv1.6 (IC_{50}~0.3 mM) channels [54, 55]. In both cases, the 4-AP block appeared to occur by means of an open-channel trapping mechanism (characterised by a decay phase resembling fast inactivation and the fact that the effect on kinetics was seen only for the first voltage pulse after application of 4-AP). This mechanism is known to be more pronounced in channels with no N-type inactivation [42]. Thus, the open-channel block by 4-AP again is consistent with the K^+ currents expressed in both cell lines inactivating mainly by a C-type mechanism.

Tetraethylammonium

The AT-2 and the MAT-LyLu cells had IC_{50} values for TEA of 9.0 and 10.6 mM, respectively, similar to those reported for Kv1.3 and 1.6 [15, 54, 55] but not Kv1.4 channels [54].

Verapamil

In both cell lines, 20 μM verapamil reduced the peak current by ~50%, increased current decay approximately tenfold but had no effect on current activation. These effects were unlikely to have been caused indirectly via voltage-gated Ca^{2+} channels, since these are not present (Y. Ding, J. Robbins, S.P. Fraser and M.B.A. Djamgoz, unpublished observations). Of the Kv1 family of K^+ channels tested for verapamil sensitivity, Kv1.3 showed an IC_{50} of 8–30 μM, comparable to the IC_{50} of ~20 μM for both AT-2 and the MAT-LyLu cell lines, but dissimilar to the IC_{50} of 708 μM for Kv1.4 [10, 32, 43].

Margatoxin

MGTX is a potent blocker of Kv1.3 and to a lesser extent Kv1.1, 1.2 and 1.6 channels [16, 17]. The IC_{50} value of <1 nM for the MGTX block of the VGPC in both AT-2 and MAT-LyLu cell lines is in the region for cloned Kv1.3 channels [17]. However, the maximal block by MGTX was 55–70%, suggesting expression of Kv subunit combinations less sensitive to MGTX in both cell lines.

Charybdotoxin

CTX blocks Ca^{2+}-dependent ('BK'-type) and Kv1.3 subtypes of VGPCs, as well as some other members of the Kv1 family, including Kv1.4 and 1.6, at higher concentrations [17, 54, 55]. The IC_{50} for CTX was in the nanomolar range for both AT-2 and MAT-LyLu cell lines, similar to Kv1.3 channels [53]. However, some 30–45% of the VGPCs was not blocked by CTX in both cell lines, suggesting expression of Kv subunit combinations less sensitive to CTX. The greater percentage (~80%) blockage of the VGPCs induced by the combined application of 4.5×10^{-8} M CTX and 5×10^{-8} M MGTX would, in addition, suggest that each cell line also contains Kv subunits or subunit combinations showing differential sensitivity to CTX and/or MGTX. However, since co-application of a 26-fold higher concentration of CTX and MGTX produced no further blockage of the

VGPCs in the MAT-LyLu cells, there must be a minority population of VGPCs expressed in both cell lines which are insensitive to these toxins.

Thus, the pharmacological data taken together are strongly supportive of (1) the majority of the outward current in both AT-2 and MAT-LyLu cell lines being due to a Kv1.3-like K^+ channel, and (2) there also being a minority sub-population of Kv subunits or Kv subunit combinations that are insensitive to both CTX and MGTX.

Possible molecular nature of the K^+ channel(s) in AT-2 and MAT-LyLu cells

The electrophysiological and pharmacological characteristics of the VGPC expressed in AT-2 and the MAT-LyLu cells were similar to Kv1.3, in terms of activation/inactivation kinetics, slow recovery from inactivation/cumulative inactivation and sensitivity to TEA, 4-AP, verapamil, MGTX and CTX. Primary cultures of rat prostate epithelial cells have also been found to express a VGPC with properties similar to Kv1.3 [38]. In addition, our Western blot and RT-PCR data indicated that some Kv1.4 and 1.6 α-subunits could be present in both cell lines. On the other hand, there was no evidence for Kv1.1, 1.2 and 1.5 α-subunit expression.

Four α-subunits must co-assemble to form a functional VGPC [39]. In the cells studied here, if the functional VGPCs consisted of homomeric-tetramers of Kv1.3, 1.4 or 1.6, then there should have been distinct channel subtypes detectable in analysis of dose-response curves, since the individual Kv1 family subunits display very different sensitivity to some of the drugs tested [54]. Furthermore, differences may have been expected in the channels' electrophysiological characteristics (e.g. kinetics). Since neither was the case, it is more likely that the VGPC α-subunits formed heteromeric assemblies [23, 46]. The overall characteristics of the resulting whole-cell current would then depend on the functional stoichiometry relevant to particular parameters. The presence of a given subunit may be sufficient to impose its particular characteristic on the whole VGPC ('dominance'), for example, channel inactivation [31], or channel characteristics may be determined either by 'blending' or 'additivity' of each subunit. Furthermore, co-expression of wild-type (inactivating) and mutant (non-inactivating) VGPC α-subunits resulted in a macroscopic current with decay characteristics described by a single exponential that would be expected from the weighted sum of the five possible channel assemblies [31]. In conclusion, therefore, the data are consistent with the majority of VGPC α-subunits of both the AT-2 and MAT-LyLu cells being a continuum of Kv1.3, 1.4 and 1.6 heteromeric assemblies, the Kv1.3 subunit probably being dominant. The presence of a single MGTX/CTX-insensitive subunit in a Kv hetero-tetramer, reducing the sensitivity of the channel to the toxins [48], could explain why (1) the block was incomplete, and (2) individual cells differed in their sensitivity to these toxins. However, we cannot rule out the possibility that other members of the Kv1 family (and/or other VGPCs) were also being expressed.

Possible relevance to metastasis

In numerous respects, the voltage-activated K^+ currents of the AT-2 and the MAT-LyLu cells appeared similar. At present, the possible functional relevance of the predominant Kv1.3 α-subunit expression particularly to cancer metastasis is not known. Lymphocytes also express mainly Kv1.3 channels and these control their activation [30]. Interestingly, activated lymphocytes and metastatic cancer cells share some functional similarities, such as intra/extravasation and ability to invade tissues during inflammatory response.

Importantly, some quantitative differences were found between the AT-2 and the MAT-LyLu cells (Table 1). In particular, compared to the AT-2 cells, the MAT-LyLu cells have (1) significantly smaller maximal K^+ current densities, and (2) a more negative resting potential. A number of minor, but still statistically significant, differences were also noted for the MAT-LyLu versus AT-2 cells as follows: (1) The slope factor for channel activation was smaller; (2) the voltage at which current was half-inactivated, and the slope factor for channel inactivation were greater; (3) the time constants for current decay at −20 and 0 mV were smaller; and (4) the residual peak current following 60 s of repetitive voltage pulses for stimulation frequencies in the range 0.05–0.2 Hz was larger.

Taken together, these characteristics would suggest that the K^+ current in the MAT-LyLu cells might be less active. This, coupled with the exclusive expression of functional VGSCs in the MAT-LyLu cell line [19], would be consistent with their 'excitability' and the possible role of VGSC activity in metastatic cell behaviour [13, 14, 19, 27, 52]. Furthermore, VGPC activity may regulate cell proliferation [5, 6, 8, 14, 37], adhesion [24], solute and water transport [25], cell volume regulation [29] and apoptosis [5].

Acknowledgements This work was supported by grants from the AICR (Association for International Cancer Research), KANCATAK and the MRC. We gratefully acknowledge the support of contributors to the Prostate Cancer Research Fund (PCRF). In addition, we thank Prof. James Trimmer for the Kv1.5 antibody, Prof. Clare Isacke for providing the secondary antibodies, Dr. N. Mohammed for help with preparation of the Western blot figure, and Dr. Jo Hirano for help with the PCR experiments.

References

1. BekeleArcuri Z, Matos MF, Manganas L, Strassle BW, Monaghan MM, Rhodes KJ, Trimmer JS (1996) Generation and characterization of subtype-specific monoclonal antibodies to K^+ channel alpha- and beta-subunit polypeptides. Neuropharmacology 35:851–865

2. Blandino JKW, Viglione MP, Bradley WA, Oie HK, Kim YI (1995) Voltage-dependent sodium channels in human small-cell lung cancer cells: role in action potentials and inhibition by Lambert-Eaton syndrome IgG. J Membr Biol 143:153–163
3. Caffrey JM, Brown AM, Schneider MD (1987) Mitogens and oncogenes can block the induction of specific voltage-gated ion channels. Science 236:570–573
4. Chen C, Corbley MJ, Roberts TM, Hess P (1988) Voltage-sensitive calcium channels in normal and transformed 3T3 fibroblasts. Science 239:1024–1026
5. Chin LS, Park CC, Zitnay KM, Sinha M, DiPatri AJ, Perillán P, Simard JM (1997) 4-aminopyridine causes apoptosis and blocks an outward rectifier K^+ channel in malignant astrocytoma cell lines. J Neurosci Res 48:122–127
6. Chiu SY, Wilson GF (1989) The role of potassium channels in Schwann cell proliferation in Wallerian degeneration of explant rabbit sciatic nerves. J Physiol (Lond) 408:199–222
7. Chomczynski P, Sacchi N (1987) Single-step method of RNA isolation by acid guanidinium thiocyanate-phenol-chloroform extraction. Anal Biochem 162:156–159
8. DeCoursey TE, Chandy KG, Gupta S, Cahalan MD (1984) Voltage-gated K^+ channels in human T lymphocytes: a role in mitogenesis. Nature 307:465–468
9. Diss JKJ, Archer SN, Hirano J, Fraser SP, Djamgoz MBA (2001) Expression profiles of voltage-gated Na^+ channel α-subunit genes rat and human prostate cancer cell lines. Prostate 48:1–14
10. Douglass J, Osborne PB, Cai YC, Wilkinson M, Christie NJ, Adelman JP (1990) Characterization and functional expression of a rat genomic DNA clone encoding a lymphocyte potassium channel. J Immunol 144:4841–4850
11. Fitzsimmons SA, Workman P, Grever M, Paull K, Camalier R, Lewis AD (1996) Reductase enzyme expression across the National Cancer Institute Tumor cell line panel: correlation with sensitivity to mitomycin C and EO9. J Natl Cancer Inst 88:259–269
12. Fraser SP, Salvador V, Djamgoz MBA (1998) Voltage-gated Na^+ channel activity contributes to rodent prostate cancer migration in vitro. J Physiol (Lond) 513:131P
13. Fraser SP, Ding Y, Liu A, Foster CS, Djamgoz MBA (1999) Tetrodotoxin suppresses morphological enhancement of the metastatic MAT-LyLu rat prostate cancer cell line. Cell Tissue Res 295:505–512
14. Fraser SP, Grimes JA, Djamgoz MBA (2000) Effects of voltage-gated ion channel modulators on rat prostatic cancer cell proliferation: comparison of strongly and weakly metastatic cell lines. Prostate 44:61–76
15. Frech GC, VanDongen AMJ, Schuster G, Brown AM, Joho RH (1989) A novel potassium channel with delayed rectifier properties isolated from rat brain by expression cloning. Nature 340:642–645
16. Garcia ML, Galvez A, Garcia-Calvo M, King VF, Vazquez J, Kaczorowski GJ (1991) Use of toxins to study potassium channels. J Bioenerg Biomembr 23:615–646
17. Garcia-Calvo M, Leonard RJ, Novick J, Stevens SP, Scmalhofer W, Kaczorowski GJ, Garcia ML (1993) Purification, characterization, and biosynthesis of margatoxin, a component of *Centruoides margaritatus* venom that selectively inhibits voltage-dependent potassium channels. J Biol Chem 268:18866–18874
18. Grimes JA, Djamgoz MBA (1998) Electrophysiological characterization of voltage-gated Na^+ current expressed in the highly metastatic Mat-LyLu cell line of rat prostate cancer. J Cell Physiol 175:50–58
19. Grimes JA, Fraser SP, Stephens GJ, Downing JEG, Laniado ME, Foster CS, Abel PD, Djamgoz MBA (1995) Differential expression of voltage-activated Na^+ currents in two prostatic tumour cell lines: contribution to invasiveness in vitro. FEBS Lett 369:290–294
20. Hamann M, Widmer H, Baroffio A, Aubry JP, Krause RM, Kaelin A, Bader CR (1994) Sodium and potassium currents in freshly isolated and in proliferating human muscle satellite cells. J Physiol (Lond) 475:305–317
21. Hille B (1992) Ionic channels of excitable membranes, 2nd edn. Sinauer, Sunderland, Mass
22. Isaacs JT, Isaacs WT, Feitz WFJ, Scheres J (1986) Establishment and characterization of seven Dunning rat prostatic cancer cell lines and their use in developing methods for predicting metastatic abilities of prostatic cancers. Prostate 9:261–281
23. Isacoff EY, Jan YN, Jan LY (1990) Evidence for the formation of heteromultimeric potassium channels in *Xenopus* oocytes. Nature 345:530–534
24. Itoh K, Stevens B, Schachner R, Fields RD (1995) Regulated expression of the neural cell adhesion molecule L1 by specific patterns of neural impulses. Science 27:1369–1372
25. Kupper J, Bowlby MR, Marom S, Levitan IB (1995) Intracellular and extracellular amino acids that influence C-type inactivation and its modulation in a voltage-dependent potassium channel. Pflugers Arch 430:1–11
26. Lang F, Rehwald W (1992) Potassium channels in renal epithelial transport regulation. Physiol Rev 72:1–32
27. Laniado ME, Lalani E-N, Fraser SP, Grimes JA, Bhangal G, Djamgoz MBA, Abel PD (1997) Expression and functional analysis of voltage-activated Na^+ channels in human prostate cancer cell lines and their contribution to invasiveness in vitro. Am J Pathol 150:1213–1221
28. Laniado ME, Fraser SP, Djamgoz MBA (2001) Voltage-gated K^+ channel activity in human prostate cancer cell lines of markedly different metastatic potential: Distinguishing characteristics of PC-3 and LNCaP cells. Prostate 45:1–15
29. Lee SC, Price M, Prystowsky MB, Deutsch C (1988) Volume response of quiescent and interleukin 2-stimulated T-lymphocytes to hypotonicity. Am J Physiol 254:C286–296
30. Levite M, Cahalon L, Peretz A, Hershkoviz R, Sobko A, Ariel A, Desai R, Attali B, Lider O (2000) Extracellular K^+ and opening of voltage-gated potassium channels activate T cell integrin function: physical and functional association between Kv1.3 channels and beta 1 integrins. J Exp Med 191:1167–1176
31. MacKinnon R, Aldrich RW, Lee AW (1993) Functional stoichiometry of Shaker potassium channel inactivation. Science 262:757–759
32. Madeja M, Müller V, Mußhoff U, Speckmann E-J (2000) Sensitivity of native and cloned hippocampal delayed rectifier potassium channels to verapamil. Neuropharmacology 39:202–210
33. Manganas LN, Trimmer JS (2000) Subunit composition determines Kv1 potassium channel surface expression. J Biol Chem 275:29685–29693
34. Marin A, Lopez de Cerain A, Hamilton E, Lewis AD, Martinez-Penuela JM, Idoate MA, Bello J (1997) DT-diaphorase and cytochrome B5 reductase in human lung and breast tumours. Br J Cancer 76:923–929
35. Marom S, Levitan IB (1994) State-dependent inactivation of the Kv3 potassium channel. Biophys J 67:579–589
36. McGee R, Sansom MSP, Usherwood PNR (1988) Characterization of a delayed rectifier K^+ channel in NG108–15 neuroblastoma×glioma cells: gating kinetics and the effects of enrichment of membrane phospholipids with arachodonic acid. J Membr Biol 102:21–34
37. Nilius B, Wohlrab W (1992) Potassium channels and regulation of proliferation of human melanoma cells. J Physiol (Lond) 445:537–548
38. Ouadid-Ahidouch H, Coppenolle FV, Bourhis XL, Belhaj A, Prevarskaya N (1999) Potassium channels in rat prostate epithelial cells. FEBS Lett 459:15–21
39. Parcej DN, Scott VE, Dolly JO (1992) Oligomeric properties of alpha-dendrotoxin-sensitive potassium ion channels purified from bovine brain. Biochemistry 31:11084–11088
40. Po S, Roberds S, Snyders DJ, Tamkun MM, Bennett PB (1993) Heteromultimeric assembly of human potassium channels. Molecular basis of a transient outward current? Circ Res 72:1326–1336

41. Rane SG (2000) The growth regulatory fibroblast IK channel is the predominant electrophysiological feature of rat prostatic cancer cells. Biochem Biophys Res Commun 269:457–463
42. Rasmusson RL, Zhang Y, Campbell DL, Comer MB, Castellino RC, Liu S, Strauss HC (1995) Bi-stable block by 4-aminopyridine of a transient K^+ channel (Kv1.4) cloned from ferret ventricle and expressed in *Xenopus* oocytes. J Physiol (Lond) 485:59–71
43. Rauer H, Grissmer S (1996) Evidence for an internal phenylalkylamine action on the voltage-gated potassium channel Kv1.3. Mol Pharmacol 50:1625–1634
44. Rettig J, Heinemann SH, Wunder F, Lorra C, Parcej DN, Dolly JO, Pongs O (1994) Inactivation properties of voltage-gated K^+ channels altered by presence of β-subunit. Nature 369:289–294
45. Roeper J, Sewing S, Zhang Y, Sommer T, Wanner SG, Pongs O (1998) NIP domain prevents N-type inactivation in voltage-gated potassium channels. Nature 391:390–393
46. Ruppersberg JP, Schroter KH, Sakmann B, Stocker M, Sewing S, Pongs O (1990) Heteromultimeric channels formed by rat brain potassium channel proteins. Nature 345:535–537
47. Ruppersberg JP, Frank R, Pongs O, Stocker M (1991) Cloned neuronal IK(A) channels reopen during recovery from inactivation. Nature 353:657–660
48. Russell SN, Overturf KE, Horowitz B (1994) Heterotetramer formation and charybdotoxin sensitivity of two K^+ channels cloned from smooth muscle. Am J Physiol 267:C1729–C1733
49. Scott VES, Muniz ZM, Sewing S, Lichtinghagen R, Parcej DN, Pongs O, Dolly JO (1994) Antibodies specific for distinct Kv subunits unveil a heterooligomeric basis for subtypes of α-dendrotoxin-sensitive K^+ channels in bovine brain. Biochem 33:1617–1623
50. Shamotienko OG, Parcej DN, Dolly JO (1997) Subunit combinations defined for K^+ channel Kv1 subtypes in synaptic membranes from bovine brain. Biochem 36:8195–8201
51. Skryma RN, Prevarskaya NB, Dufy-Barbe L, Odessa MF, Audin J, Dufy B (1997) Potassium conductance in the androgen-sensitive prostate cancer cell line, LNCaP: involvement in cell proliferation. Prostate 33:112–122
52. Smith P, Rhodes NP, Shortland AP, Fraser SP, Djamgoz MBA, Ke Y, Foster CS (1998) Sodium channel protein expression enhances the invasiveness of rat and human prostate cancer cells. FEBS Lett 423:19–24
53. Spencer RH, Sokolov Y, Li H, Takenaka B, Milici AJ, Aiyar J, Nguyen A, Park H, Jap BK, Hall JE, Gutman GA, Chandy KG (1997) Purification, visualization, and biophysical characterization of Kv1.3 tetramers. J Biol Chem 272:2389–2395
54. Stühmer W, Ruppersberg JP, Schroter KH, Sakmann B, Stocker M, Giese KP, Perschke A, Baumann A, Pongs O (1989) Molecular basis of functional diversity of voltage-gated potassium channels in mammalian brain. EMBO J 8:3235–3244
55. Swanson R, Marshall J, Smith JS, Williams JB, Boyle MB, Folander K, Luneau CJ, Antanavage J, Oliva C, Buhrow SA, Bennett C, Stein RB, Kaczmarek LK (1990) Cloning and expression of cDNA and genomic clones encoding three delayed rectifier potassium channels in rat brain. Neuron 4:929–939